

## Bending and free vibration analysis for FGM plates containing various distribution shape of porosity

Lazreg Hadji<sup>\*1,2</sup>, Fabrice Bernard<sup>3</sup>,  
Abdelkader Safa<sup>4</sup> and Abdelouahed Tounsi<sup>5,6,7</sup>

<sup>1</sup> Department of Mechanical Engineering, University of Tiaret, BP 78 Zaaroura, Tiaret (14000), Algeria

<sup>2</sup> Laboratory of Geomatics and Sustainable Development, University of Tiaret, Algeria

<sup>3</sup> University of Rennes, INSA Rennes, Laboratory of Civil Engineering and Mechanical Engineering, France

<sup>4</sup> Department of Civil Engineering, Ahmed Zabana University Centre, Relizane, 48000, Algeria

<sup>5</sup> Material and Hydrology Laboratory, Faculty of Technology, Civil Engineering Department, University of Sidi Bel Abbes, Algeria

<sup>6</sup> YFL (Yonsei Frontier Lab), Yonsei University, Seoul, Korea

<sup>7</sup> Department of Civil and Environmental Engineering, King Fahd University of Petroleum & Minerals, 31261 Dhahran, Eastern Province, Saudi Arabia

(Received July 26, 2020, Revised March 1, 2021, Accepted March 22, 2021)

**Abstract.** In this paper hyperbolic shear deformation plate theory is presented for bending and the free vibration of functionally graded plates with considering porosities that may possibly occur inside the functionally graded materials (FGMs) during their fabrication. Four different porosity types are used for functionally graded plates. Equations of motion are derived from Hamilton's principle. In the solution of the governing equations, the Navier procedure is implemented. In the numerical examples, the effects of the porosity parameters, porosity types and geometry parameters on the bending and free vibration of the functionally graded plates are investigated. It was found that the distribution form of porosity significantly influence the mechanical behavior of FG plates, in terms of deflection, normal, shear stress and frequency.

**Keywords:** bending; free vibration; functionally graded materials; porosity; Hamilton's principle

### 1. Introduction

Functionally graded materials (FGMs) are a novel class of engineering materials which have been developed by combining dissimilar materials to possess smooth variation of material properties along the desired direction(s). FGMs have great potential for improving material/structural performance in many engineering applications precisely because of their spatially graded heterogeneous micro structure.

In the production stage of the functionally graded materials, micro-voids and porosities could occur due to production or technical errors. With porosity, the mechanical behavior of functionally graded materials changes considerably. Thus, the effect of the porosity on the functionally graded materials is an important problem and must be investigated in order to safe design of this

---

\*Corresponding author, Ph.D., E-mail: [had\\_laz@yahoo.fr](mailto:had_laz@yahoo.fr)

composites.

In last years, lots of researchers focus on investigation of porous functionally graded materials; Wattanasakulpong and Ungbhakorn (2014) studied vibration characteristics of FGM porous beams by using differential transformation method with different kinds of elastic supports. Akbaş (2015) investigated wave propagation of a functionally graded beam in thermal environments. Ebrahimi *et al.* (2017) investigated the thermo-mechanical vibration analysis of functionally graded micro/nanoscale beams with porosities based on modified couple stress theory. Akbaş (2017a, b, c, d) examined the static, buckling and vibration of functionally graded beams with porosity. Akbaş (2017e) used generalized differential quadrature method for stability of a non-homogenous porous plate. Jouneghani *et al.* (2018) studied analytically the structural response of porous FGM nonlocal nanobeams under hygro-thermo-mechanical loadings. Wu *et al.* (2018) performed a finite element analysis to study the free and forced vibration FGM porous beam using both Euler-Bernoulli and Timoshenko beam theories. Akbaş (2018a) examined forced vibration analysis of functionally graded porous deep beams. Akbaş (2018b) developed geometrically nonlinear analysis of functionally graded porous beams. Hadj *et al.* (2019) studied the influence of the distribution shape of porosity on the bending FGM new plate model resting on elastic foundations. Avcar (2019) examined the free vibration of functionally graded beams with porosity with different porosity distribution models. Bourada *et al.* (2019) investigated the dynamic of porous functionally graded beam using a sinusoidal shear deformation theory. Akbaş (2019a, b) developed hygro-thermal post-buckling and Hygro-thermal nonlinear analysis of a functionally graded beam. Akbaş (2019c) studied buckling analysis of a fiber reinforced laminated composite plate with porosity. Akbaş (2019d) analyzed longitudinal forced vibration of porous a nanorod. Xu *et al.* (2019) studied buckling analysis of functionally graded porous plates with laminated face sheets by using finite element method based on first order shear deformation theory. Zhao *et al.* (2019) investigated vibration behavior of the FGM porous curved thick beam, doubly-curved panels and shells of revolution by using a semi-analytical method. Ramteke *et al.* (2019) studied effects of the porosity on the eigen characteristics of functionally graded structures with different types of porosity and material distributions. Akbaş (2020a) analyze dynamic of thick beams with functionally graded porous layers and viscoelastic support. Akbaş (2020b) studied dynamic analysis of viscoelastic functionally graded porous thick beams under pulse load. Trinh *et al.* (2019) studied the effects of porosity and thermomechanical loading on free vibration and nonlinear dynamic response of functionally graded sandwich shells with double curvature. Trinh *et al.* (2020) used a semi-analytical stochastic buckling quantification of porous functionally graded plates. Nguyen *et al.* (2020) investigated nonlinear buckling and post-buckling analysis of shear deformable stiffened truncated conical sandwich shells with functionally graded face sheets and a functionally graded porous core.

This work aims to use a hyperbolic shear deformation theory to study the effect of the distribution form of porosity on bending and free vibration behavior of FGM plates. The effect due to porosity is included using a modified mixture law covering the porosity phases proposed by Wattanasakulpong *et al.* (2012), Demirhan and Taskin (2019) and Younsi *et al.* (2018). The distinctive feature of this study from published papers in the literature is to investigate the porous functionally graded plates with four porosity types and higher-order shear deformation plate theory. The effects of the porosity parameters, porosity types and aspect ratio of plates on the normal stress, shear stress, static deflections and frequency are presented and discussed.

## 2. Geometric configuration and material properties

Consider a FG rectangular plate occupying the region  $r$  from the coordinate system  $(x; y; z)$  as shown in Fig. 1. This plate is made of an isotropic material with material properties varying smoothly in the  $z$  (thickness) direction only. We assume that the composition is varied from the bottom to the top surfaces, i.e., the bottom surface ( $z = -h/2$ ) of the plate is metal rich whereas the top surface ( $z = +h/2$ ) is ceramic-rich.

In this study, we consider an imperfect FGM plate with a volume fraction of porosity  $\alpha$  ( $\alpha \ll 1$ ) with different form of distribution between the metal and the ceramic. The modified mixture rule proposed by Wattanasakulpong and Ungbhakornb (2014) is

$$P(z) = P_m \left( V_m - \frac{\alpha}{2} \right) + P_c \left( V_c - \frac{\alpha}{2} \right) \tag{1}$$

The power law of the volume fraction of the ceramic is assumed as

$$V_c = \left( \frac{z}{h} + \frac{1}{2} \right)^k \tag{2}$$

The modified mixture rule becomes

$$P(z) = (P_c - P_m) \left( \frac{z}{h} + \frac{1}{2} \right)^k + P_m - (P_c + P_m) \frac{\alpha}{2} \tag{3}$$

Where,  $k$  is the power law index that takes values greater than or equals to zero. The FGM plaque becomes a fully ceramic beam when  $k$  is set to zero and fully metal for large value of  $k$ .

The mechanical properties of FGM such as Young's modulus  $E$  and mass density  $\rho$  of the imperfect FG can be written as a functions of thickness coordinate  $z$  (middle surface), as follows (Atmane *et al.* 2015, Daouadji and Benferhat 2016, Hadji and Adda Bedia 2015).

$$E(z) = (E_c - E_m) \left( \frac{z}{h} + \frac{1}{2} \right)^k + E_m - (E_c + E_m) \frac{\alpha}{2} \tag{4b}$$

$$\rho(z) = (\rho_c - \rho_m) \left( \frac{z}{h} + \frac{1}{2} \right)^k + \rho_m - (\rho_c + \rho_m) \frac{\alpha}{2} \tag{4a}$$

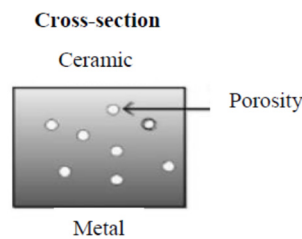


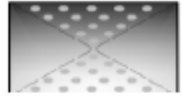



Fig. 1 Geometry of rectangular FG plate and coordinates

Table 1 Different distribution forms of porosity (Hadj *et al.* 2019)

Distribution forms of porosity	Elastic modulus expression	Schema
Homogeneous shape	$E(z) = (E_c - E_m) \left( \frac{z}{h} + \frac{1}{2} \right)^k + E_m - (E_c + E_m) \frac{\alpha}{2}$	
Form "O" shape	$E(z) = (E_c - E_m) \left( \frac{z}{h} + \frac{1}{2} \right)^k + E_m - (E_c + E_m) \frac{\alpha}{2} \left( 1 - 2 \frac{ z }{h} \right)$	
Form "X" shape	$E(z) = (E_c - E_m) \left( \frac{z}{h} + \frac{1}{2} \right)^k + E_m - (E_c + E_m) \frac{\alpha}{2} \left( 2 \frac{z}{h} \right)$	
Form "V" shape	$E(z) = (E_c - E_m) \left( \frac{z}{h} + \frac{1}{2} \right)^k + E_m - (E_c + E_m) \frac{\alpha}{2} \left( \frac{1}{2} + \frac{z}{h} \right)$	

The material properties of a perfect FGM plate can be obtained when the volume fraction of porosity  $\alpha$  is set to zero. Due to the small variations of the Poisson ratio  $\nu$ , it is assumed to be constant. Several porosity distributions have been studied in the present work, such as "O", "V" and "X" (Table 1).

### 3. Kinematic, strain and stress relations

The displacement field, taking into account the shear deformation effect, is presented for FGM structures as Hadji *et al.* (2011)

$$\begin{aligned}
 U(x, y, z, t) &= u_0(x, y, t) - z \frac{\partial w_b}{\partial x} - f(z) \frac{\partial w_s}{\partial x} \\
 V(x, y, z, t) &= v_0(x, y, t) - z \frac{\partial w_b}{\partial y} - f(z) \frac{\partial w_s}{\partial y} \\
 W(x, y, z, t) &= w_b(x, y, t) + w_s(x, y, t)
 \end{aligned} \tag{5}$$

where  $u_0$  and  $v_0$  are the mid-plane displacements of the plate in the  $x$  and  $y$  directions, respectively;  $w_b$  and  $w_s$  are the bending and shear components of transverse displacement, respectively. It should be noted that unlike the FSDT, this theory does not require shear correction factors.

The shape function proposed by Akavci (HSDPT) (Akavci 2010) based on the hyperbolic function is used in this work.

$$f(z) = z \left[ 1 + \frac{3\pi}{2} \operatorname{sech} \left( \frac{1}{2} \right)^2 \right] - \frac{3\pi}{2} h \tanh \left( \frac{z}{h} \right) \tag{6}$$

It can be seen that the displacement field in Eq. (5) introduces only four unknowns ( $u_0$ ,  $v_0$ ,  $w_b$  and  $w_s$ ). The nonzero strains associated with the displacement field in Eq. (4) are

$$\begin{Bmatrix} \gamma_{yz} \\ \gamma_{xz} \end{Bmatrix} = g(z) \begin{Bmatrix} \gamma_{yz}^s \\ \gamma_{xz}^s \end{Bmatrix}, \quad \begin{Bmatrix} \varepsilon_x \\ \varepsilon_y \\ \gamma_{xy} \end{Bmatrix} = \begin{Bmatrix} \varepsilon_x^0 \\ \varepsilon_y^0 \\ \gamma_{xy}^0 \end{Bmatrix} + z \begin{Bmatrix} k_x^b \\ k_y^b \\ k_{xy}^b \end{Bmatrix} + f(z) \begin{Bmatrix} k_x^s \\ k_y^s \\ k_{xy}^s \end{Bmatrix} \quad (7)$$

where

$$\begin{Bmatrix} \varepsilon_x^0 \\ \varepsilon_y^0 \\ \gamma_{xy}^0 \end{Bmatrix} = \begin{Bmatrix} \frac{\partial u_0}{\partial x} \\ \frac{\partial v_0}{\partial x} \\ \frac{\partial u_0}{\partial y} + \frac{\partial v_0}{\partial x} \end{Bmatrix}, \quad \begin{Bmatrix} k_x^b \\ k_y^b \\ k_{xy}^b \end{Bmatrix} = \begin{Bmatrix} -\frac{\partial^2 w_b}{\partial x^2} \\ -\frac{\partial^2 w_b}{\partial y^2} \\ -2\frac{\partial^2 w_b}{\partial x \partial y} \end{Bmatrix}, \quad (8a)$$

$$\begin{Bmatrix} k_x^s \\ k_y^s \\ k_{xy}^s \end{Bmatrix} = \begin{Bmatrix} -\frac{\partial^2 w_s}{\partial x^2} \\ -\frac{\partial^2 w_s}{\partial y^2} \\ -2\frac{\partial^2 w_s}{\partial x \partial y} \end{Bmatrix}, \quad \begin{Bmatrix} \gamma_{yz}^s \\ \gamma_{xz}^s \end{Bmatrix} = \begin{Bmatrix} \frac{\partial w_s}{\partial y} \\ \frac{\partial w_s}{\partial x} \end{Bmatrix}$$

and

$$g(z) = 1 - \frac{df(z)}{dz} \quad (8b)$$

The linear constitutive relations of a FG plate can be written as

$$\begin{Bmatrix} \sigma_x \\ \sigma_y \\ \tau_{xy} \end{Bmatrix} = \begin{bmatrix} Q_{11} & Q_{12} & 0 \\ Q_{12} & Q_{22} & 0 \\ 0 & 0 & Q_{66} \end{bmatrix} \begin{Bmatrix} \varepsilon_x \\ \varepsilon_y \\ \gamma_{xy} \end{Bmatrix} \quad \text{and} \quad \begin{Bmatrix} \tau_{yz} \\ \tau_{zx} \end{Bmatrix} = \begin{bmatrix} Q_{44} & 0 \\ 0 & Q_{55} \end{bmatrix} \begin{Bmatrix} \gamma_{yz} \\ \gamma_{zx} \end{Bmatrix} \quad (9)$$

where

$$Q_{11} = Q_{22} = \frac{E(z)}{1-\nu^2}, \quad Q_{12} = \frac{\nu E(z)}{1-\nu^2}, \quad Q_{44} = Q_{55} = Q_{66} = \frac{E(z)}{2(1+\nu)} \quad (10)$$

#### 4. Equations of motion

Hamilton's principle is herein utilized to determine the equations of motion

$$0 = \int_0^t (\delta U + \delta V - \delta T) dt \quad (11)$$

where  $\delta U$  is the variation of strain energy;  $\delta T$  is the variation of kinetic energy; and  $\delta V$  is the

variation of work done.

The variation of strain energy of the plate is given by

$$\begin{aligned} \delta U &= \int_V [\sigma_x \delta \varepsilon_x + \sigma_y \delta \varepsilon_y + \tau_{xy} \delta \gamma_{xy} + \tau_{yz} \delta \gamma_{yz} + \tau_{xz} \delta \gamma_{xz}] dV \\ &= \int_A [N_x \delta \varepsilon_x^0 + N_y \delta \varepsilon_y^0 + N_{xy} \delta \gamma_{xy}^0 + M_x^b \delta k_x^b + M_y^b \delta k_y^b + M_{xy}^b \delta k_{xy}^b \\ &\quad + M_x^s \delta k_x^s + M_y^s \delta k_y^s + M_{xy}^s \delta k_{xy}^s + S_{yz}^s \delta \gamma_{yz}^s + S_{xz}^s \delta \gamma_{xz}^s] dA = 0 \end{aligned} \quad (12)$$

where  $A$  is the top surface and the stress resultants  $N$ ,  $M$ , and  $S$  are defined by

$$(N_i, M_i^b, M_i^s) = \int_{-\frac{h}{2}}^{\frac{h}{2}} (1, z, f) \sigma_i dz \quad (i = x, y, xy) \quad \text{and} \quad (S_{xz}^s, S_{yz}^s) = \int_{-\frac{h}{2}}^{\frac{h}{2}} g(\tau_{xz}, \tau_{yz}) dz \quad (13)$$

The variation of kinetic energy of the plate can be expressed as

$$\begin{aligned} \delta T &= \int_{-\frac{h}{2}}^{\frac{h}{2}} \int_{\Omega} [\dot{u} \delta \dot{u} + \dot{v} \delta \dot{v} + \dot{w} \delta \dot{w}] \rho(z) d\Omega dz \\ &= \int_A \{ I_0 [\dot{u}_0 \delta \dot{u}_0 + \dot{v}_0 \delta \dot{v}_0 + (\dot{w}_b + \dot{w}_s)(\delta \dot{w}_b + \delta \dot{w}_s)] \\ &\quad - I_1 \left( \dot{u}_0 \frac{\partial \delta \dot{w}_b}{\partial x} + \frac{\partial \dot{w}_b}{\partial x} \delta \dot{u}_0 + \dot{v}_0 \frac{\partial \delta \dot{w}_b}{\partial y} + \frac{\partial \dot{w}_b}{\partial y} \delta \dot{v}_0 \right) \\ &\quad - I_2 \left( \dot{u}_0 \frac{\partial \delta \dot{w}_s}{\partial x} + \frac{\partial \dot{w}_s}{\partial x} \delta \dot{u}_0 + \dot{v}_0 \frac{\partial \delta \dot{w}_s}{\partial y} + \frac{\partial \dot{w}_s}{\partial y} \delta \dot{v}_0 \right) \\ &\quad + J_1 \left( \frac{\partial \dot{w}_b}{\partial x} \frac{\partial \delta \dot{w}_b}{\partial x} + \frac{\partial \dot{w}_b}{\partial y} \frac{\partial \delta \dot{w}_b}{\partial y} \right) + K_2 \left( \frac{\partial \dot{w}_s}{\partial x} \frac{\partial \delta \dot{w}_s}{\partial x} + \frac{\partial \dot{w}_s}{\partial y} \frac{\partial \delta \dot{w}_s}{\partial y} \right) \\ &\quad + J_2 \left( \frac{\partial \dot{w}_b}{\partial x} \frac{\partial \delta \dot{w}_s}{\partial x} + \frac{\partial \dot{w}_s}{\partial x} \frac{\partial \delta \dot{w}_b}{\partial x} + \frac{\partial \dot{w}_b}{\partial y} \frac{\partial \delta \dot{w}_s}{\partial y} + \frac{\partial \dot{w}_s}{\partial y} \frac{\partial \delta \dot{w}_b}{\partial y} \right) \} d\Omega \end{aligned} \quad (14)$$

Where dot-superscript convention indicates the differentiation with respect to the time variable  $t$ ;  $\rho(z)$  is the mass density given by Eq. (4b); and  $(I_i, J_i, K_i)$  are mass inertias expressed by

$$(I_0, I_1, I_2) = \int_{-\frac{h}{2}}^{\frac{h}{2}} (1, z, z^2) \rho(z) dz \quad (15a)$$

$$(J_1, J_2, K_2) = \int_{-\frac{h}{2}}^{\frac{h}{2}} (f, z f, f^2) \rho(z) dz \quad (15b)$$

The variation of work done can be expressed as

$$\delta V = - \int_A q \delta W dA \quad (16)$$

By substituting Eqs. (12), (14) and (16) into Eq. (11), the following can be derived:

$$\begin{aligned}
\delta u_0: \quad & \frac{\partial N_x}{\partial x} + \frac{\partial N_{xy}}{\partial y} = I_0 \ddot{u}_0 - I_1 \frac{\partial \ddot{w}_b}{\partial x} - J_1 \frac{\partial \ddot{w}_s}{\partial x} \\
\delta v_0: \quad & \frac{\partial N_{xy}}{\partial x} + \frac{\partial N_y}{\partial y} = I_0 \ddot{v}_0 - I_1 \frac{\partial \ddot{w}_b}{\partial y} - J_1 \frac{\partial \ddot{w}_s}{\partial y} \\
\delta w_b: \quad & \frac{\partial^2 M_x^b}{\partial x^2} + 2 \frac{\partial^2 M_{xy}^b}{\partial x \partial y} + \frac{\partial^2 M_y^b}{\partial y^2} + q \\
& = I_0 (\ddot{w}_b + \ddot{w}_s) + I_1 \left( \frac{\partial \ddot{u}_0}{\partial x} + \frac{\partial \ddot{v}_0}{\partial y} \right) - I_2 \nabla^2 \ddot{w}_b - J_2 \nabla^2 \ddot{w}_s \\
\delta w_s: \quad & \frac{\partial^2 M_x^s}{\partial x^2} + 2 \frac{\partial^2 M_{xy}^s}{\partial x \partial y} + \frac{\partial^2 M_y^s}{\partial y^2} + \frac{\partial S_{xz}^s}{\partial x} + \frac{\partial S_{yz}^s}{\partial y} + q \\
& = I_0 (\ddot{w}_b + \ddot{w}_s) + J_1 \left( \frac{\partial \ddot{u}_0}{\partial x} + \frac{\partial \ddot{v}_0}{\partial y} \right) - J_2 \nabla^2 \ddot{w}_b - K_2 \nabla^2 \ddot{w}_s
\end{aligned} \tag{17}$$

Substituting Eq. (7) into Eq. (9) and the subsequent results into Eq. (13), the stress resultants are obtained in terms of strains as following compact form:

$$\begin{Bmatrix} N \\ M^b \\ M^s \end{Bmatrix} = \begin{bmatrix} A & B & B^s \\ B & D & D^s \\ B^s & D^s & H^s \end{bmatrix} \begin{Bmatrix} \varepsilon \\ k^b \\ k^s \end{Bmatrix}, \quad S = A^s \gamma, \tag{18}$$

in which

$$N = \{N_x, N_y, N_{xy}\}^t, \quad M^b = \{M_x^b, M_y^b, M_{xy}^b\}^t, \quad M^s = \{M_x^s, M_y^s, M_{xy}^s\}^t, \tag{19a}$$

$$\varepsilon = \{\varepsilon_x^0, \varepsilon_y^0, \gamma_{xy}^0\}^t, \quad k^b = \{k_x^b, k_y^b, k_{xy}^b\}^t, \quad k^s = \{k_x^s, k_y^s, k_{xy}^s\}^t, \tag{19b}$$

$$A = \begin{bmatrix} A_{11} & A_{12} & 0 \\ A_{12} & A_{22} & 0 \\ 0 & 0 & A_{66} \end{bmatrix}, \quad B = \begin{bmatrix} B_{11} & B_{12} & 0 \\ B_{12} & B_{22} & 0 \\ 0 & 0 & B_{66} \end{bmatrix}, \quad D = \begin{bmatrix} D_{11} & D_{12} & 0 \\ D_{12} & D_{22} & 0 \\ 0 & 0 & D_{66} \end{bmatrix}, \tag{19c}$$

$$B^s = \begin{bmatrix} B_{11}^s & B_{12}^s & 0 \\ B_{12}^s & B_{22}^s & 0 \\ 0 & 0 & B_{66}^s \end{bmatrix}, \quad D^s = \begin{bmatrix} D_{11}^s & D_{12}^s & 0 \\ D_{12}^s & D_{22}^s & 0 \\ 0 & 0 & D_{66}^s \end{bmatrix}, \quad H^s = \begin{bmatrix} H_{11}^s & H_{12}^s & 0 \\ H_{12}^s & H_{22}^s & 0 \\ 0 & 0 & H_{66}^s \end{bmatrix}, \tag{19d}$$

$$S = \{S_{xz}^s, S_{yz}^s\}^t, \quad \gamma = \{\gamma_{xz}^s, \gamma_{yz}^s\}^t, \quad A^s = \begin{bmatrix} A_{44}^s & 0 \\ 0 & A_{55}^s \end{bmatrix}, \tag{19e}$$

and stiffness components are given as

$$\begin{Bmatrix} A_{11} & B_{11} & D_{11} & B_{11}^s & D_{11}^s & H_{11}^s \\ A_{12} & B_{12} & D_{12} & B_{12}^s & D_{12}^s & H_{12}^s \\ A_{66} & B_{66} & D_{66} & B_{66}^s & D_{66}^s & H_{66}^s \end{Bmatrix} = \int_{-h/2}^{h/2} Q_{11}(1, z, z^2, f(z), z f(z), f^2(z)) \begin{Bmatrix} 1 \\ \nu \\ \frac{1-\nu}{2} \end{Bmatrix} dz \tag{20a}$$

$$(A_{22}, B_{22}, D_{22}, B_{22}^s, D_{22}^s, H_{22}^s) = (A_{11}, B_{11}, D_{11}, B_{11}^s, D_{11}^s, H_{11}^s) \quad (20b)$$

$$A_{44}^s = A_{55}^s = \int_{-h/2}^{h/2} Q_{44}[g(z)]^2 dz, \quad (20c)$$

Introducing Eq. (18) into Eq. (17), the equations of motion can be expressed in terms of displacements ( $u_0$ ,  $v_0$ ,  $w_b$ ,  $w_s$ ) and the appropriate equations take the form

$$\begin{aligned} & (A_{12} + A_{66}) \frac{\partial^2 u}{\partial x \partial y} + A_{66} \frac{\partial^2 v}{\partial x^2} + A_{22} \frac{\partial^2 v}{\partial y^2} - (B_{12} + 2B_{66}) \frac{\partial^3 w_b}{\partial x^2 \partial y} - B_{22} \frac{\partial^3 w_b}{\partial y^3} \\ & - B_{22}^s \frac{\partial^3 w_s}{\partial y^3} - (B_{12}^s + 2B_{66}^s) \frac{\partial^3 w_s}{\partial x^2 \partial y} = I_0 \ddot{v}_0 - I_1 \frac{\partial \ddot{w}_b}{\partial y} - J_1 \frac{\partial \ddot{w}_s}{\partial y} \end{aligned} \quad (21a)$$

$$\begin{aligned} & (A_{12} + A_{66}) \frac{\partial^2 u}{\partial x \partial y} + A_{66} \frac{\partial^2 v}{\partial x^2} + A_{22} \frac{\partial^2 v}{\partial y^2} - (B_{12} + 2B_{66}) \frac{\partial^3 w_b}{\partial x^2 \partial y} - B_{22} \frac{\partial^3 w_b}{\partial y^3} \\ & - B_{22}^s \frac{\partial^3 w_s}{\partial y^3} - (B_{12}^s + 2B_{66}^s) \frac{\partial^3 w_s}{\partial x^2 \partial y} = I_0 \ddot{v}_0 - I_1 \frac{\partial \ddot{w}_b}{\partial y} - J_1 \frac{\partial \ddot{w}_s}{\partial y} \end{aligned} \quad (21b)$$

$$\begin{aligned} & B_{11} \frac{\partial^3 u}{\partial x^3} + (B_{12} + 2B_{66}) \frac{\partial^3 u}{\partial x \partial y^2} + (B_{12} + 2B_{66}) \frac{\partial^3 v}{\partial x^2 \partial y} + B_{22} \frac{\partial^3 v}{\partial y^3} - D_{11} \frac{\partial^4 w_b}{\partial x^4} \\ & - 2(D_{12} + 2D_{66}) \frac{\partial^4 w_b}{\partial x^2 \partial y^2} - D_{22} \frac{\partial^4 w_b}{\partial y^4} - D_{11}^s \frac{\partial^4 w_s}{\partial x^4} - 2(D_{12}^s + 2D_{66}^s) \frac{\partial^4 w_s}{\partial x^2 \partial y^2} \\ & - D_{22}^s \frac{\partial^4 w_s}{\partial y^4} + q = I_0 (\ddot{w}_b + \ddot{w}_s) + I_1 \left( \frac{\partial \ddot{u}_0}{\partial x} + \frac{\partial \ddot{v}_0}{\partial y} \right) - I_2 \nabla^2 \ddot{w}_b - J_2 \nabla^2 \ddot{w}_s, \end{aligned} \quad (21c)$$

$$\begin{aligned} & B_{11}^s \frac{\partial^3 u}{\partial x^3} + (B_{12}^s + 2B_{66}^s) \frac{\partial^3 u}{\partial x \partial y^2} + (B_{12}^s + 2B_{66}^s) \frac{\partial^3 v}{\partial x^2 \partial y} + B_{22}^s \frac{\partial^3 v}{\partial y^3} - D_{11}^s \frac{\partial^4 w_b}{\partial x^4} \\ & - 2(D_{12}^s + 2D_{66}^s) \frac{\partial^4 w_b}{\partial x^2 \partial y^2} - D_{22}^s \frac{\partial^4 w_b}{\partial y^4} - H_{11}^s \frac{\partial^4 w_s}{\partial x^4} - 2(H_{12}^s + 2H_{66}^s) \frac{\partial^4 w_s}{\partial x^2 \partial y^2} \\ & - H_{22}^s \frac{\partial^4 w_s}{\partial y^4} + A_{55}^s \frac{\partial^2 w_s}{\partial x^2} + A_{44}^s \frac{\partial^2 w_s}{\partial y^2} + q \\ & = I_0 (\ddot{w}_b + \ddot{w}_s) + J_1 \left( \frac{\partial \ddot{u}_0}{\partial x} + \frac{\partial \ddot{v}_0}{\partial y} \right) - J_2 \nabla^2 \ddot{w}_b - K_2 \nabla^2 \ddot{w}_s \end{aligned} \quad (21d)$$

Clearly, when the effect of transverse shear deformation is neglected  $w_s$ , Eq. (20) yields the equations of motion of FG plate based on the CPT.

## 5. Navier solution for simply supported rectangular plates

The Navier solution method is employed to determine the analytical solutions for which the displacement variables are written as product of arbitrary parameters and known trigonometric functions to respect the equations of motion and boundary conditions.



$$\begin{Bmatrix} u_0 \\ v_0 \\ w_b \\ w_s \end{Bmatrix} = \sum_{m=1}^{\infty} \sum_{n=1}^{\infty} \begin{Bmatrix} U_{mn} e^{i\omega t} \cos(\lambda x) \sin(\mu y) \\ V_{mn} e^{i\omega t} \sin(\lambda x) \cos(\mu y) \\ W_{bmn} e^{i\omega t} \sin(\lambda x) \sin(\mu y) \\ W_{smn} e^{i\omega t} \sin(\lambda x) \sin(\mu y) \end{Bmatrix} \quad (22)$$

where  $U_{mn}$ ;  $V_{mn}$ ;  $W_{bmn}$ ; and  $W_{smn}$  are arbitrary parameters to be determined,  $\omega$  is the eigenfrequency associated with the  $(m, n)$ th eigenmode, and  $\lambda = m\pi/a$  and  $\mu = n\pi/b$ .

The transverse load  $q$  is also expanded in the double-Fourier sine series as

$$q(x, y) = \sum_{m=1}^{\infty} \sum_{n=1}^{\infty} q_{mn} \sin(\lambda x) \sin(\mu y) \quad (23)$$

For the case of a sinusoidally distributed load, we have

$$m = n = 1 \quad \text{and} \quad q_{11} = q_0 \quad (24)$$

where  $q_0$  represents the intensity of the load at plate centre.

Substituting Eqs. (22) and (23) into Eq. (21), the following problem is obtained:

$$\begin{pmatrix} S_{11} & S_{12} & S_{13} & S_{14} \\ S_{12} & S_{22} & S_{23} & S_{24} \\ S_{13} & S_{23} & S_{33} & S_{34} \\ S_{14} & S_{24} & S_{34} & S_{44} \end{pmatrix} - \omega^2 \begin{pmatrix} m_{11} & 0 & 0 & 0 \\ 0 & m_{22} & 0 & 0 \\ 0 & 0 & m_{33} & m_{34} \\ 0 & 0 & m_{34} & m_{44} \end{pmatrix} \begin{Bmatrix} U_{mn} \\ V_{mn} \\ W_{bmn} \\ W_{smn} \end{Bmatrix} = \begin{Bmatrix} 0 \\ 0 \\ q_{mn} \\ q_{mn} \end{Bmatrix} \quad (25)$$

where

$$\begin{cases} S_{11} = A_{11}\lambda^2 + A_{66}\mu^2, \\ S_{12} = \lambda\mu(A_{12} + A_{66}) \\ S_{13} = -\lambda(B_{11}\lambda^2 + (B_{12} + 2B_{66})\mu^2), \\ S_{14} = -\lambda(B_{11}^s\lambda^2 + (B_{12}^s + 2B_{66}^s)\mu^2), \\ S_{22} = A_{66}\lambda^2 + A_{22}\mu^2, \\ S_{23} = -\mu((B_{12} + 2B_{66})\lambda^2 + B_{22}\mu^2), \\ S_{24} = -\mu((B_{12}^s + 2B_{66}^s)\lambda^2 + B_{22}^s\mu^2), \\ S_{33} = D_{11}\lambda^4 + 2(D_{12} + 2D_{66})\lambda^2\mu^2 + D_{22}\mu^4, \\ S_{34} = D_{11}^s\lambda^4 + 2(D_{12}^s + 2D_{66}^s)\lambda^2\mu^2 + D_{22}^s\mu^4, \\ S_{44} = H_{11}^s\lambda^4 + 2(H_{12}^s + 2H_{66}^s)\lambda^2\mu^2 + H_{22}^s\mu^4 + A_{55}^s\lambda^2 + A_{44}^s\mu^2, \\ m_{11} = m_{22} = I_1, \\ m_{33} = I_0 + I_2(\lambda^2 + \mu^2), \\ m_{34} = I_0 + J_2(\lambda^2 + \mu^2), \\ m_{44} = I_0 + K_2(\lambda^2 + \mu^2), \end{cases} \quad (26)$$

## 6. Results and discussion

In this study, the bending and free vibration analysis of FG plates by the new hyperbolic shear deformation plate theory is suggested for investigation, the effect of the distribution form of porosity is also studied; the Poisson's ratio is fixed at  $\nu = 0.3$ . Comparisons are made with the solutions available in the literature in order to verify the accuracy of this analysis.

### 6.1 Static analysis

For static analysis the plates are subjected to a sinusoidal distributed transverse load given by

$$q(x, y) = q_{11} \sin(\lambda x) \sin(\mu y) \quad (27)$$

A functionally graded material consisting of Aluminum- Alumina is considered. The following material properties are used in computing the numerical values.

$$\begin{aligned} \text{Metal (Aluminum, Al)} \quad E_m &= 70 \text{ GPa}, \quad \text{Poisson's ratio } (\nu) = 0.3. \\ \text{Ceramic (Alumina, Al}_2\text{O}_3) \quad E_c &= 380 \text{ GPa}, \quad \text{Poisson's ratio } (\nu) = 0.3. \end{aligned}$$

Results are tabulated in Tables 2 and 3. The tables contain the non dimensionalised deflections and stresses respectively.

In order to prove the validity of the presented higher-order shear deformation plate theory, some comparisons are made between the results obtained from this theory and those obtained by a generalized shear deformation theory developed by Zenkour (2006), the Zeroth order Shear Deformation Theory (ZSDT) (Dharan *et al.* 2010) and the results obtained by the model of Reddy's based on the HSDT (Reddy 2000). The uniform distribution shape of porosity are considered. The following non dimensionalised quantities are reported.

$$\begin{aligned} \bar{W} &= 10 \frac{E_c h^3}{q_0 a^4} w \left( \frac{a}{2}, \frac{b}{2} \right), & \bar{U} &= 100 \frac{E_c h^3}{q_0 a^4} u \left( 0, \frac{b}{2}, \frac{-h}{4} \right), & \bar{V} &= 100 \frac{E_c h^3}{q_0 a^4} v \left( \frac{a}{2}, 0, \frac{-h}{6} \right), \\ \bar{\sigma}_x &= \frac{h}{hq_0} \sigma_x \left( \frac{a}{2}, \frac{b}{2}, \frac{h}{2} \right), & \bar{\sigma}_y &= \frac{h}{hq_0} \sigma_y \left( \frac{a}{2}, \frac{b}{2}, \frac{h}{3} \right), & \bar{\tau}_{xy} &= \frac{h}{hq_0} \tau_{xy} \left( 0, 0, \frac{h}{3} \right), \\ \bar{\tau}_{xz} &= \frac{h}{hq_0} \tau_{xz} \left( 0, \frac{b}{2}, 0 \right), & \bar{\tau}_{yz} &= \frac{h}{hq_0} \tau_{yz} \left( \frac{a}{2}, 0, \frac{h}{6} \right), \end{aligned}$$

Table 2 Effects of Volume fraction exponent on the dimensionless displacements of a FGM square plate subjected to sinusoidal loading ( $a/h = 10$ )

$k$	Model	$\alpha$	$\bar{U}$	$\bar{V}$	$\bar{W}$	
Ceramic	ZSDT (Dharan <i>et al.</i> 2010)	$\alpha = 0$	0.21805	0.14493	0.29423	
	GSDT (Zenkour 2006)	$\alpha = 0$	0.23090	0.15390	0.29600	
	HSDT (Reddy 2000)	$\alpha = 0$	0.21805	0.14493	0.29423	
	Present		$\alpha = 0$	0.21816	0.14489	0.29604
			$\alpha = 0.1$	0.23189	0.15400	0.31468
			$\alpha = 0.2$	0.24746	0.16435	0.33581

Table 2 Continued

$k$	Model	$\alpha$	$\bar{U}$	$\bar{V}$	$\bar{W}$
0.2	ZSDT (Dharan <i>et al.</i> 2010)	$\alpha = 0$	0.2818	0.1985	0.33672
	GSDT (Zenkour 2006)	$\alpha = 0$	-	-	-
	HSDT (Reddy 2000)	$\alpha = 0$	0.28172	0.19820	0.33767
	Present	$\alpha = 0$	0.30479	0.21539	0.35988
		$\alpha = 0.1$	0.33202	0.23552	0.38827
0.5	Present	$\alpha = 0.2$	0.36454	0.25971	0.42162
		ZSDT (Dharan <i>et al.</i> 2010)	$\alpha = 0$	0.42135	0.31096
	GSDT (Zenkour 2006)	$\alpha = 0$	-	-	-
	HSDT (Reddy 2000)	$\alpha = 0$	0.42131	0.31034	0.44407
	Present	$\alpha = 0$	0.43859	0.32549	0.45369
$\alpha = 0.1$		0.49628	0.37089	0.50253	
$\alpha = 0.2$		0.57114	0.43023	0.56405	
1	ZSDT (Dharan <i>et al.</i> 2010)	$\alpha = 0$	0.64258	0.49673	0.59059
	GSDT (Zenkour 2006)	$\alpha = 0$	0.6626	0.5093	0.5889
	HSDT (Reddy 2000)	$\alpha = 0$	0.64137	0.49438	0.58895
	Present	$\alpha = 0$	0.64112	0.49408	0.58893
		$\alpha = 0.1$	0.77156	0.60065	0.68318
$\alpha = 0.2$		0.96748	0.76194	0.81924	
2	ZSDT (Dharan <i>et al.</i> 2010)	$\alpha = 0$	0.9022	0.71613	0.76697
	GSDT (Zenkour 2006)	$\alpha = 0$	0.92810	0.73110	0.75730
	HSDT (Reddy 2000)	$\alpha = 0$	0.89858	0.71035	0.75747
	Present	$\alpha = 0$	0.89793	0.70968	0.75733
		$\alpha = 0.1$	1.18383	0.94886	0.94196
$\alpha = 0.2$		1.73521	1.41394	1.28005	
5	ZSDT (Dharan <i>et al.</i> 2010)	$\alpha = 0$	1.06786	0.84942	0.94325
	GSDT (Zenkour 2006)	$\alpha = 0$	1.11580	0.87920	0.91180
	HSDT (Reddy 2000)	$\alpha = 0$	1.06297	0.84129	0.90951
	Present	$\alpha = 0$	1.06620	0.84399	0.91171
		$\alpha = 0.1$	1.52547	1.23283	1.19970
$\alpha = 0.2$		2.70313	2.24280	1.87542	
Metallic	ZSDT (Dharan <i>et al.</i> 2010)	$\alpha = 0$	1.18373	0.78677	1.59724
	GSDT (Zenkour 2006)	$\alpha = 0$	1.25340	0.83560	1.6070
	HSDT (Reddy 2000)	$\alpha = 0$	1.18373	0.78677	1.59724
	Present	$\alpha = 0$	1.18429	0.78652	1.60709
		$\alpha = 0.1$	1.74527	1.15909	2.36835
$\alpha = 0.2$		3.31601	2.20227	4.49987	

Table 3 Effects of Volume fraction exponent on the dimensionless stresses of a FGM square plate subjected to sinusoidal loading ( $a/h = 10$ )

$k$	Model	$\alpha$	$\bar{\sigma}_x$	$\bar{\sigma}_y$	$\bar{\tau}_{xy}$	$\bar{\tau}_{xz}$	$\bar{\tau}_{yz}$
Ceramic	ZSDT (Dharan <i>et al.</i> 2010)	$\alpha = 0$	1.98915	1.31035	0.70557	0.23778	0.23778
	GSDT (Zenkour 2006)	$\alpha = 0$	1.9955	1.3121	0.7065	0.2462	0.2132
	HSDT (Reddy 2000)	$\alpha = 0$	1.98915	1.31035	0.70557	0.23778	0.19051
	Present	$\alpha = 0$	1.99515	1.31219	0.70656	0.24406	0.21289
		$\alpha = 0.1$	1.99515	1.31219	0.70656	0.24406	0.21289
		$\alpha = 0.2$	1.99515	1.31219	0.70656	0.24406	0.21289
0.2	ZSDT (Dharan <i>et al.</i> 2010)	$\alpha = 0$	2.1227	1.30962	0.6678	0.22557	0.2256
	GSDT (Zenkour 2006)	$\alpha = 0$	-	-	-	-	-
	HSDT (Reddy 2000)	$\alpha = 0$	2.12671	1.30958	0.66757	0.22532	0.18045
	Present	$\alpha = 0$	2.26003	1.38706	0.72053	0.24805	0.22655
		$\alpha = 0.1$	2.28168	1.39323	0.72174	0.24836	0.22755
		$\alpha = 0.2$	2.30723	1.40051	0.72317	0.24872	0.22871
0.5	ZSDT (Dharan <i>et al.</i> 2010)	$\alpha = 0$	2.60436	1.47175	0.66709	0.23909	0.23869
	GSDT (Zenkour 2006)	$\alpha = 0$	-	-	-	-	-
	HSDT (Reddy 2000)	$\alpha = 0$	2.61051	1.47147	0.66668	0.23817	0.19071
	Present	$\alpha = 0$	2.61929	1.45863	0.69119	0.24945	0.24311
		$\alpha = 0.1$	2.68941	1.47532	0.68966	0.24997	0.24577
		$\alpha = 0.2$	2.77837	1.49653	0.68775	0.25061	0.24896
1	ZSDT (Dharan <i>et al.</i> 2010)	$\alpha = 0$	3.07011	1.48935	0.61395	0.22705	0.23919
	GSDT (Zenkour 2006)	$\alpha = 0$	3.087	1.4894	0.611	0.2462	0.2622
	HSDT (Reddy 2000)	$\alpha = 0$	3.08501	1.4898	0.61111	0.23817	0.19071
	Present	$\alpha = 0$	3.08640	1.4895	0.61106	0.24406	0.26178
		$\alpha = 0.1$	3.26288	1.5185	0.59549	0.24406	0.26721
		$\alpha = 0.2$	3.51847	1.5604	0.57289	0.24406	0.27399
2	ZSDT (Dharan <i>et al.</i> 2010)	$\alpha = 0$	3.58089	1.3968	0.54947	0.22705	0.22719
	GSDT (Zenkour 2006)	$\alpha = 0$	3.6094	1.3954	0.5441	0.2265	0.2763
	HSDT (Reddy 2000)	$\alpha = 0$	3.60664	1.39575	0.54434	0.22568	0.1807
	Present	$\alpha = 0$	3.60856	1.39561	0.54413	0.22427	0.27558
		$\alpha = 0.1$	3.96831	1.41036	0.50721	0.22074	0.28539
		$\alpha = 0.2$	4.61670	1.43564	0.44023	0.21543	0.29843
5	ZSDT (Dharan <i>et al.</i> 2010)	$\alpha = 0$	4.19547	1.1087	0.57811	0.21792	0.21813
	GSDT (Zenkour 2006)	$\alpha = 0$	4.2488	1.1029	0.5755	0.2017	0.2429
	HSDT (Reddy 2000)	$\alpha = 0$	4.24293	1.10539	0.57368	0.21609	0.17307
	Present	$\alpha = 0$	4.24758	1.10329	0.57553	0.19919	0.24164
		$\alpha = 0.1$	4.74916	1.03851	0.55112	0.18612	0.25074
		$\alpha = 0.2$	5.78994	0.88676	0.50484	0.16142	0.26720

Table 3 Continued

$k$	Model	$\alpha$	$\bar{\sigma}_x$	$\bar{\sigma}_y$	$\bar{\tau}_{xy}$	$\bar{\tau}_{xz}$	$\bar{\tau}_{yz}$	
Metallic	ZSDT (Dharan <i>et al.</i> 2010)	$\alpha = 0$	1.98915	1.31035	0.70557	0.23778	0.23778	
	GSDT (Zenkour 2006)	$\alpha = 0$	1.9955	1.3121	0.7065	0.2462	0.2132	
	HSDT (Reddy 2000)	$\alpha = 0$	1.98915	1.31035	0.70557	0.23778	0.19051	
	Present		$\alpha = 0$	1.99515	1.31219	0.70656	0.24406	0.21289
			$\alpha = 0.1$	1.99515	1.31219	0.70656	0.24406	0.21289
			$\alpha = 0.2$	1.99515	1.31219	0.70656	0.24406	0.21289

As we can see on Tables 2 and 3, close agreements were obtained between the results of the present theory and those of literature (when  $\alpha = 0$ ; perfect plate). The tables shows the effect of volume fraction exponent ( $V_f$ ) on the stresses and displacements of a functionally graded square plate with  $a/h = 10$ . It can be observed that as the plate becomes more and more metallic the deflection  $\bar{W}$  and normal stress  $\bar{\sigma}_x$  increases but normal stress  $\bar{\sigma}_y$  decreases. It is very interesting to note that the stresses for a fully ceramic plate are the same as that of a fully metal plate. This is due to the fact that in these two cases the plate is fully homogeneous and stresses do not depend on the modulus of elasticity. By introducing the volume fraction of porosity ( $\alpha$ ), it can be noted that the increase of this factor induces an increase in dimensionless deflections, displacements and stresses which shows that the porosity has a significant influence on the displacements and stress of FGM plates.

Fig. 2 indicates the effect the aspect ratio  $a/b$  and the shape of porosity distribution on the dimensionless deflections of FGM plates, made with Al/Al<sub>2</sub>O<sub>3</sub>. The porosity coefficient  $\alpha = 0.2$ . As we can seen on Fig. 3, the dimensionless deflections decrease in increasing the aspect ratio  $a/b$ . The deflections for plate with uniform porosity distribution model are higher than that for the other models of imperfect FGM plates. The highest values of dimensionless deflections were obtained for the homogeneous shape of porosity distribution while the lowest ones correspond to the "X"

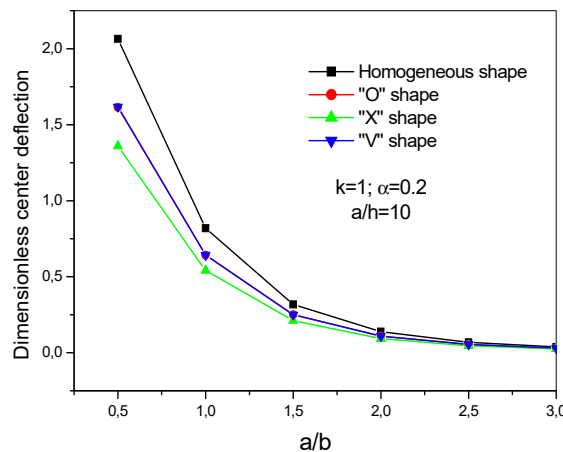


Fig. 2 Effect of the shape of porosity distribution on the dimensionless deflections versus aspect ratio ( $a/b$ ) of an Al/Al<sub>2</sub>O<sub>3</sub> FGM plate ( $k = 1$ ;  $\alpha = 0.2$ )

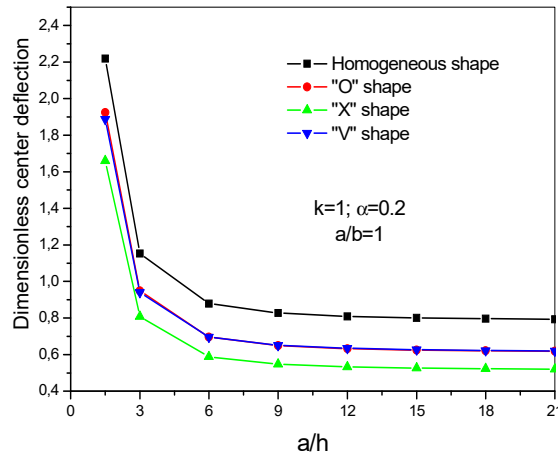


Fig. 3 Effect of the shape of porosity distribution on the dimensionless deflections versus side-to-thickness ratio ( $a/h$ ) of an Al/Al<sub>2</sub>O<sub>3</sub> FGM square plate ( $k = 1$ ;  $\alpha = 0.2$ )

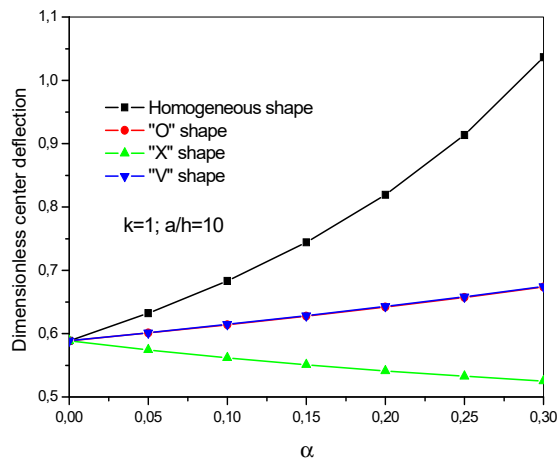


Fig. 4 Effect of porosity coefficient on center deflection FGM square plate ( $k = 1$ )

shape of porosity distribution. The "V" and the "O" shape of porosity distribution gives almost the same values of the dimensionless deflections. Another result of Fig. 2 is that the difference among of porosity distributions decrease significantly by increasing the ratio of  $a/b$ .

In Fig. 3, we present the effect of the distribution shape of porosity on the dimensionless deflections of FGM square plate for different side to thickness ratio  $a/h$ , made with Al/Al<sub>2</sub>O<sub>3</sub>. It should be noted that the effect of the distribution shape of porosity on the dimensionless deflection is very significant by increasing thickness ratio (as the plate becomes thinner). According to these figures, it is clear that the deflections is maximum for "H" distribution shape of porosity and it is minimal for "X" distribution shape of porosity. The "V" and the "O" shape of porosity distribution give almost the same values of the dimensionless deflections.

The variation of porosity coefficient  $\alpha$  on the central deflection is illustrated in Fig. 4. The porosity coefficient has an important effect on the deflections mainly for the homogeneous shape

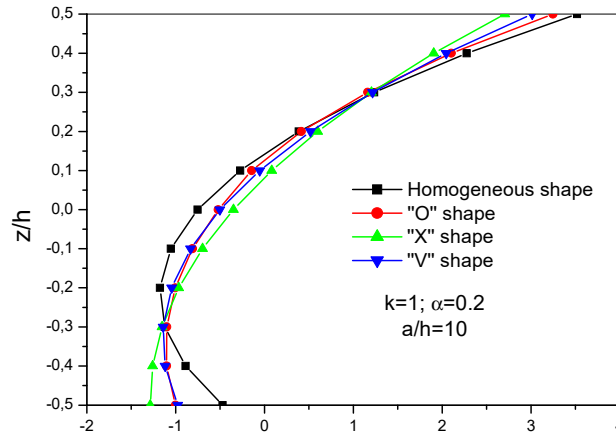


Fig. 5 Effect of the shape of porosity distribution on the normal stress  $\bar{\sigma}_{xx}$  across the thickness an Al/Al<sub>2</sub>O<sub>3</sub> FGM square plate ( $a/h = 10$ ;  $\alpha = 0.2$ )

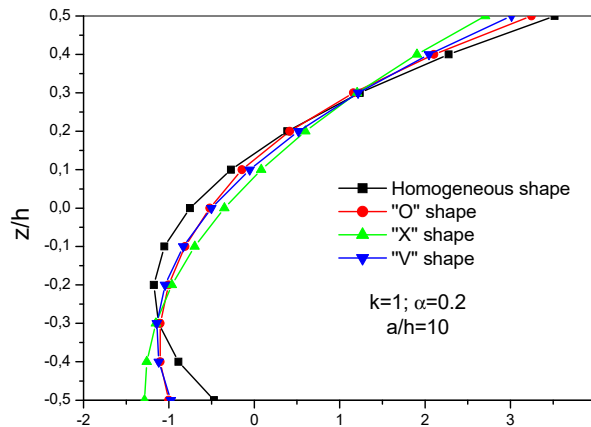


Fig. 6 Effect of the shape of porosity distribution on the normal stress  $\bar{\sigma}_{yy}$  across the thickness an Al/Al<sub>2</sub>O<sub>3</sub> FGM square plate ( $a/h = 10$ ;  $\alpha = 0.2$ )

of porosity distribution where the increasing of porosity coefficient increases the central deflections. With increasing of the porosity parameters, the difference among of porosity distributions increases considerably.

Figs. 5 and 6 shows the influence of distribution shape of porosity on the axial stress with porosity coefficient  $\alpha = 0.2$ . According to these figures, it is clear that the longitudinal stress is maximum for “H” distribution shape of porosity and it is minimal for “X” distribution shape of porosity.

Figs. 7 to 9 shows the influence of distribution shape of porosity on the shear stress with porosity coefficient  $\alpha = 0.2$ . It’s clear that the distributions are not parabolic. Also, the shear stress is maximum for H distribution shape of porosity and it is minimal for “X” shape of porosity distribution.

## 6.2 Dynamic analysis

The accuracy of the present theory is also investigated through free vibration analysis of FGM porous plates. The material properties used in the present study are

$$\begin{aligned} \text{Metal (Aluminum, Al):} \quad & E_m = 70 \times 10^9 \text{ N/m}^2, \quad \nu = 0.3, \quad \rho_m = 2702 \text{ Kg/m}^3. \\ \text{Ceramic (Zirconia, ZrO}_2\text{):} \quad & E_c = 200 \times 10^9 \text{ N/m}^2, \quad \nu = 0.3, \quad \rho_c = 5700 \text{ Kg/m}^3. \end{aligned}$$

In order to validate proposed theory, a comparison study is performed. Several parameters are varied and their dynamic behavior is studied. In the validation study, the first three natural frequencies for the fundamental vibration mode of  $m = n = 1$  with different side to thickness ratio  $a/h$  are presented and compared with the results obtained from this theory and those obtained

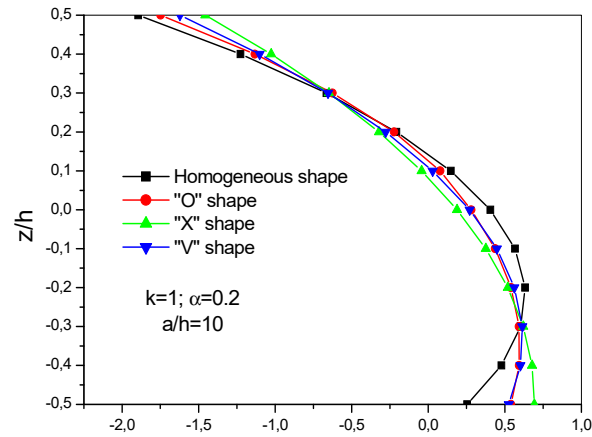


Fig. 7 Effect of the shape of porosity distribution on the shear stress  $\bar{\tau}_{xy}$  across the thickness an Al/Al<sub>2</sub>O<sub>3</sub> FGM square plate ( $a/h = 10$ ;  $\alpha = 0.2$ )

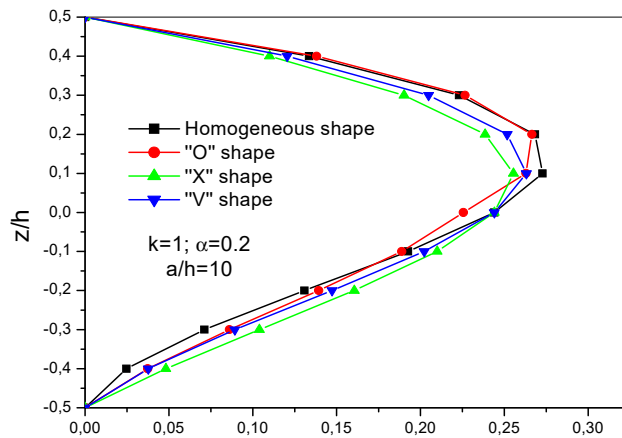


Fig. 8 Effect of the shape of porosity distribution on the shear stress  $\bar{\tau}_{xz}$  across the thickness an Al/Al<sub>2</sub>O<sub>3</sub> FGM square plate ( $a/h = 10$ ;  $\alpha = 0.2$ )



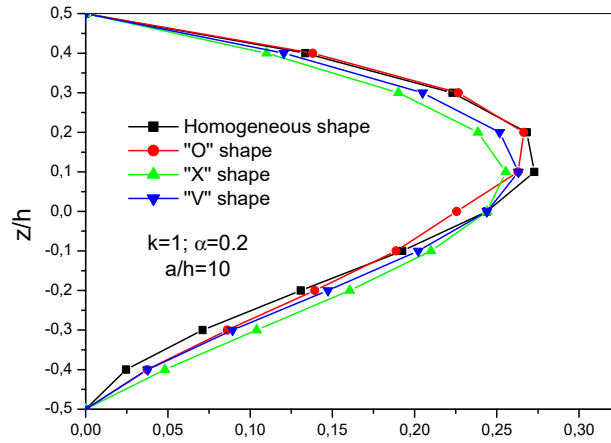


Fig. 9 Effect of the shape of porosity distribution on the shear stress  $\bar{\tau}_{xz}$  across the thickness an Al/Al<sub>2</sub>O<sub>3</sub> FGM square plate ( $a/h = 10$ ;  $\alpha = 0.2$ )

Table 4 Comparison of First Three natural frequencies of Al/ZrO<sub>2</sub> FG square plates for various a/h ratio

$$\bar{\omega} = \left( \omega \left( \frac{a^2}{h} \right) \sqrt{\frac{\rho_m}{E_m}} \right), k = 1$$

$a/h$	Theory	$\alpha$	Mode No.		
			1	2	3
5	ZSDT (Dharan <i>et al.</i> 2010)	$\alpha = 0$	5.6554	15.2996	25.9247
	HSDT (Reddy 2000)	$\alpha = 0$	5.6914	15.3408	25.9257
	HSDT2 (Nguyen <i>et al.</i> 2008)	$\alpha = 0$	5.7123	15.339	25.776
	Present	$\alpha = 0$	5.6777	15.3438	25.776
		$\alpha = 0.1$	5.9337	16.1738	27.1444
		$\alpha = 0.2$	6.2278	17.1549	28.7561
10	ZSDT	$\alpha = 0$	6.18	30.6643	51.8649
	HSDT (Reddy 2000)	$\alpha = 0$	6.1863	30.6861	51.8665
	HSDT2 (Nguyen <i>et al.</i> 2008)	$\alpha = 0$	6.1932	30.685	51.795
	Present	$\alpha = 0$	6.1813	30.6876	51.7915
		$\alpha = 0.1$	6.4985	32.3475	54.5798
		$\alpha = 0.2$	6.8700	34.3097	57.8731
20	ZSDT	$\alpha = 0$	6.3359	61.3633	103.7394
	HSDT (Reddy 2000)	$\alpha = 0$	6.3371	61.3744	103.7404
	HSDT2 (Nguyen <i>et al.</i> 2008)	$\alpha = 0$	6.339	61.374	103.71
	Present	$\alpha = 0$	6.3358	61.3751	103.7029
		$\alpha = 0.1$	6.6738	64.6951	109.3058
		$\alpha = 0.2$	7.0724	68.6195	115.9276

by the results of the Zeroth order Shear Deformation Theory (ZSDT) (Dharan *et al.* 2010), the model of Reddy's based on the HSDT, and the First order shear deformation plate models developed by Nguyen *et al.* (2008). It is seen from Table 4, a good agreement between the results of the present theory with other theories. Close agreements were obtained between the results of the present theory and those of literature (when; perfect plate). By introducing the volume fraction of porosity ( $\alpha$ ), it can be noted that the increase of this factor induces an increase in natural frequencies which shows that the porosity has a significant influence on the frequency of FGM plates.

In Fig. 10, the relationship between side-to-thickness  $a/h$  and fundamental frequency is presented for different porosity models for different schemes of layers for  $k = 2$  and  $\alpha = 0.2$ . It is

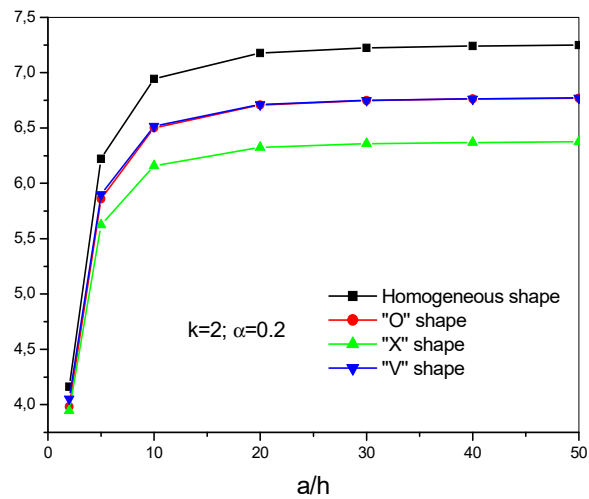


Fig. 10 Effect of the shape of porosity distribution on the dimensionless fundamental frequency  $\bar{\omega}$  versus side-to-thickness  $a/h$  of an FGM square plate ( $k = 2$ )

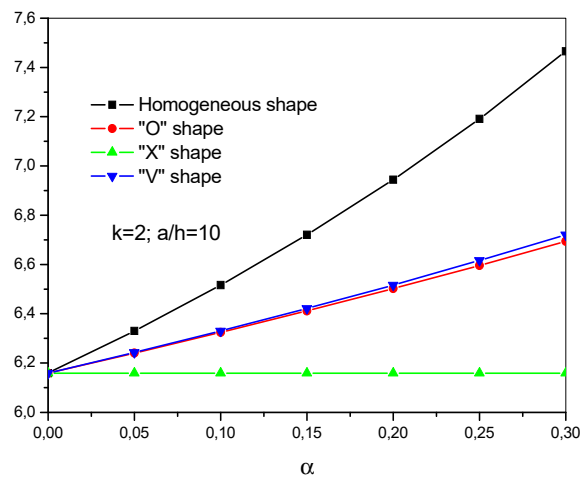


Fig. 11 Effect of porosity coefficient on the dimensionless fundamental frequency  $\bar{\omega}$  of FGM plate ( $k = 2$ )

seen from Fig. 10 that the difference among the porosity models increases with increasing of  $a/h$  ratio. In higher values of  $a/h$ , the porosity distributions play important role on the free vibration behavior of FGM porous plates. The fundamental frequency of homogeneous shape of porosity distribution are biggest values. The “V” and “O” porosity model gives almost the same frequency values. Also, the result of the X porosity model gives lowest values of fundamental frequency. The reason of this situation is that the void more stack in the X porosity distribution, and so the rigidity of the plates is lowest in the X porosity model. As a result, X porosity model gives lowest the fundamental frequency in contrast with other porosity models.

Fig. 11 shows the effects of porosity coefficient ( $\alpha$ ) on the dimensionless fundamental frequencies for  $k = 2$  and  $a/h = 10$ . As seen from Fig. 11, increasing the porosity coefficient yields to increase the difference among of porosity models, significantly and the results of V and O porosity models are very close.

## 7. Conclusions

The study was focused on the effect of the distribution shape of porosity on bending and free vibration of FGM plate by using hyperbolic shear deformation theory. Four type porosity models are used. In the solution of the problem, the Navier method is used. Effects of porosity coefficient, porosity models, FGM distribution parameter, side-to-thickness ratio on the bending and free vibration of FGM plates are investigated. It is obtained from the numerical results the side-to-thickness ratio is very influences on the porosity effects for FGM plates. Also, it can be concluded that distribution shape of porosity has a significant effect on the deflections of FGM plates as well as on the normal and shear stress developed in the plate.

Finally, it is up to the researchers and manufacturer to choose wisely the material combinations that gives rise to a fgm plate offers rigidity, strength and most of all less greedy in terms of cost. In view of this research, it is very important to study the effect of boundary conditions, and to see how these boundary conditions can affect the stability of this type of porous plate.

## Acknowledgments

This research was supported by the Algerian Ministry of Higher Education and Scientific Research (MESRS) as part of the grant for the PRFU research project n° A01L02UN140120180001 and by the University of Tiaret, in Algeria

## References

- Akavci, S.S. (2010), “Two new hyperbolic shear displacement models for orthotropic laminated composite plates”, *Mech. Compos. Mater.*, **46**, 215-226. <https://doi.org/10.1007/s11029-010-9140-3>
- Akbaş, Ş.D. (2015), “Wave propagation of a functionally graded beam in thermal environments”, *Steel Compos. Struct., Int. J.*, **19**(6), 1421-1447. <https://doi.org/10.12989/scs.2015.19.6.1421>
- Akbaş, Ş.D. (2017a), “Vibration and static analysis of functionally graded porous plates”, *J. Appl. Computat. Mech.*, **3**(3), 199-207. <https://doi.org/10.22055/JACM.2017.21540.1107>
- Akbaş, Ş.D. (2017b), “Thermal effects on the vibration of functionally graded deep beams with porosity”, *Int. J. Appl. Mech.*, **9**(5), 1750076. <https://doi.org/10.1142/S1758825117500764>

- Akbaş, Ş.D. (2017c), "Post-buckling responses of functionally graded beams with porosities", *Steel Compos. Struct., Int. J.*, **24**(5), 579-589. <https://doi.org/10.12989/scs.2017.24.5.579>
- Akbaş, Ş.D. (2017d), "Nonlinear static analysis of functionally graded porous beams under thermal effect", *Coupl. Syst. Mech., Int. J.*, **6**(4), 399-415. <https://doi.org/10.12989/csm.2017.6.4.399>
- Akbaş, Ş.D. (2017e) "Stability of a non-homogenous porous plate by using generalized differential quadrature method", *Int. J. Eng. Appl. Sci.*, **9**(2), 147-155. <https://doi.org/10.24107/ijeas.322375>
- Akbaş, Ş.D. (2018a), "Forced vibration analysis of functionally graded porous deep beams", *Compos. Struct.*, **186**, 293-302. <https://doi.org/10.1016/j.compstruct.2017.12.013>
- Akbaş, Ş.D. (2018b), "Geometrically nonlinear analysis of functionally graded porous beams", *Wind Struct., Int. J.*, **27**(1), 59-70. <https://doi.org/10.12989/was.2018.27.1.059>
- Akbaş, Ş.D. (2019a), "Hygro-thermal post-buckling analysis of a functionally graded beam", *Coupl. Syst. Mech., Int. J.*, **8**(5), 459-471. <https://doi.org/10.12989/csm.2019.8.5.459>
- Akbaş, Ş.D. (2019b), "Hygro-thermal nonlinear analysis of a functionally graded beam", *J. Appl. Computat. Mech.*, **5**(2), 477-485. <https://doi.org/10.22055/JACM.2018.26819.1360>
- Akbaş, Ş.D. (2019c), "Buckling analysis of a fiber reinforced laminated composite plate with porosity", *J. Computat. Appl. Mech.*, **50**(2), 375-380. <https://doi.org/10.22059/JCAMECH.2019.291967.448>
- Akbaş, Ş.D. (2019d), "Longitudinal forced vibration analysis of porous a nanorod", *Mühendislik Bilimleri ve Tasarım Dergisi*, **7**(4), 736-743. <https://doi.org/10.21923/jesd.553328>
- Akbaş, Ş.D. (2020a), "Dynamic analysis of thick beams with functionally graded porous layers and viscoelastic support", *J. Vib. Control*, **27**(13-14), 1644-1655. <https://doi.org/10.1177/1077546320947302>
- Akbaş, Ş.D. (2020b), "Dynamic analysis of viscoelastic functionally graded porous thick beams under pulse load", *Eng. Comput.* <https://doi.org/10.1007/s00366-020-01070-3>
- Al-Furjan, M.S.H., Habibi, M., won Jung, D., Sadeghi, S., Safarpour, H., Tounsi, A. and Chen, G. (2020a), "A computational framework for propagated waves in a sandwich doubly curved nanocomposite panel", *Eng. Comput.* <https://doi.org/10.1007/s00366-020-01130-8>
- Atmane, H.A., Tounsi, A. and Bernard, F. (2015), "Effect of thickness stretching and porosity on mechanical response of a functionally graded beams resting on elastic foundations", *Int. J. Mech. Mater.*, **13**(1), 71-84. <https://doi.org/10.1007/s10999-015-9318-x>
- Avcar, M. (2019), "Free vibration of imperfect sigmoid and power law functionally graded beams", *Steel Compos. Struct., Int. J.*, **30**(6), 603-615. <https://doi.org/10.12989/scs.2019.30.6.603>
- Bourada, F., Bousahla, A.A., Bourada, M., Azzaz, A., Zinata, A. and Tounsi, A. (2019), "Dynamic investigation of porous functionally graded beam using a sinusoidal shear deformation theory", *Wind Struct., Int. J.*, **28**(1), 19-30. <https://doi.org/10.12989/was.2019.28.1.019>
- Daouadji, T.H. and Benferhat, R. (2016), "Bending analysis of an imperfect FGM plates under hygro-thermo-mechanical loading with analytical validation", *Adv. Mater. Res., Int. J.*, **5**(1), 35-53. <https://doi.org/10.12989/amr.2016.5.1.035>
- Demirhan, P.A. and Taskin, V. (2019), "Bending and free vibration analysis of Levy-type porous functionally graded plate using state space approach", *Compos. B Eng.*, **160**, 661-676. <https://doi.org/10.1016/j.compositesb.2018.12.020>
- Dharan, S., Syam Prakash, V. and Savithri, S. (2010), "A higher order shear deformation model for functionally graded plates", *Proceedings of International Conference on Technological Trends (ICTT-2010)*, Trivandrum, India, November.
- Ebrahimi, F., Mahmoodi, F. and Barati, M.R. (2017), "Thermo-mechanical vibration analysis of functionally graded micro/nanoscale beams with porosities based on modified couple stress theory", *Adv. Mater. Res., Int. J.*, **6**(3), 279-301. <https://doi.org/10.12989/amr.2017.6.3.279>
- Hadji, L. and Adda Bedia, E.A. (2015), "Influence of the porosities on the free vibration of FGM beams", *Wind Struct., Int. J.*, **21**(3), 273-287. <https://doi.org/10.12989/was.2015.21.3.273>
- Hadji, L., Atmane, H.A., Tounsi, A., Mechab, I. and Bedia, E.A. (2011), "Free vibration of functionally graded sandwich plates using four-variable refined plate theory", *Appl. Mathe. Mech.*, **32**(7), 925-942. <https://doi.org/10.1007/s10483-011-1470-9>
- Hadji, B., Rabia, B. and Daouadji, T.H. (2019), "Influence of the distribution shape of porosity on the

- bending FGM new plate model resting on elastic foundations”, *Struct. Eng. Mech., Int. J.*, **72**(1), 823-832. <https://doi.org/10.12989/sem.2019.72.1.061>
- Hussain, M., Naeem, M.N., Khan, M.S. and Tounsi, A. (2020), “Computer-aided approach for modelling of FG cylindrical shell sandwich with ring supports”, *Comput. Concrete, Int. J.*, **25**(5), 411-425. <https://doi.org/10.12989/cac.2020.25.5.411>
- Jouneghani, F.Z., Dimitri, R. and Tornabene, F. (2018), “Structural response of porous FG nanobeams under hygro-thermo-mechanical loadings”, *Compos. Part B: Eng.*, **152**, 71-78. <https://doi.org/10.1016/j.compositesb.2018.06.023>
- Nguyen, T.K., Sab, K. and Bonnet, G. (2008), “First order shear deformation plate models for functionally graded materials”, *Compos. Struct.*, **83**, 25-36. <https://doi.org/10.1016/j.compstruct.2007.03.004>
- Nguyen, D.D., Kim, S.E. and Nguyen, D.K. (2020), “Nonlinear buckling and post-buckling analysis of shear deformable stiffened truncated conical sandwich shells with functionally graded face sheets and a functionally graded porous core”, *J. Sandw. Struct. Mater.* <https://doi.org/10.1177/1099636220906821>
- Ramteke, P.M., Panda, S.K. and Sharma, N. (2019), “Effect of grading pattern and porosity on the eigen characteristics of porous functionally graded structure”, *Steel Compos. Struct., Int. J.*, **33**(6), 865-875. <https://doi.org/10.12989/scs.2019.33.6.865>
- Reddy, J.N. (2000), “Analysis of functionally graded plates”, *Int. J. Numer. Method. Eng.*, **47**(1-3), 663-684. [https://doi.org/10.1002/\(SICI\)1097-0207\(20000110/30\)47:1/3<663::AID-NME787>3.0.CO;2-8](https://doi.org/10.1002/(SICI)1097-0207(20000110/30)47:1/3<663::AID-NME787>3.0.CO;2-8)
- Trinh, C.M., Nguyen, D.D. and Kim, S.E. (2019), “Effects of porosity and thermomechanical loading on free vibration and nonlinear dynamic response of functionally graded sandwich shells with double curvature”, *Aerosp. Sci. Technol.*, **87**, 119-132. <https://doi.org/10.1016/j.ast.2019.02.010>
- Trinh, M.C., Mukhopadhyay, T. and Kim, S.E. (2020), “A semi-analytical stochastic buckling quantification of porous functionally graded plates”, *Aerosp. Sci. Technol.*, **105**, 105928. <https://doi.org/10.1016/j.ast.2020.105928>
- Wattanasakulponga, N. and Ungbhakornb, V. (2014), “Linear and non linear vibration analysis of elastically restrained ends FGM beams with porosities”, *Aero. Sci. Technol.*, **32**(1), 111-120. <https://doi.org/10.1016/j.ast.2013.12.002>
- Wattanasakulpong, N., Prusty, B.G., Kelly, D.W. and Hoffman, M. (2012), “Free vibration analysis of layered functionally graded beams with experimental validation”, *Mater. Des.*, **36**, 182-190. <https://doi.org/10.1016/j.matdes.2011.10.049>
- Wu, D., Liu, A., Huang, Y., Huang, Y., Pi, Y. and Gao, W. (2018), “Dynamic analysis of functionally graded porous structures through finite element analysis”, *Eng. Struct.*, **165**, 287-301. <https://doi.org/10.1016/j.engstruct.2018.03.023>
- Xu, K., Yuan, Y. and Li, M. (2019), “Buckling behavior of functionally graded porous plates integrated with laminated composite faces sheets”, *Steel Compos. Struct., Int. J.*, **32**(5), 633-642. <https://doi.org/10.12989/scs.2019.32.5.633>
- Younsi, A., Tounsi, A., Zaoui, F.Z., Bousahla, A.A. and Mahmoud, S.R. (2018), “Novel quasi-3D and 2D shear deformation theories for bending and free vibration analysis of FGM plates”, *Geomech. Eng., Int. J.*, **14**(6), 519-532. <https://doi.org/10.12989/gae.2018.14.6.519>
- Zenkour, A.M. (2006), “Generalised shear deformation theory for bending analysis of functionally graded plates”, *Appl. Mathe. Modell.*, **30**, 67-84. <https://doi.org/10.1016/j.apm.2005.03.009>
- Zhao, J., Xie, F., Wang, A., Shuai, C., Tang, J. and Wang, Q. (2019), “Vibration behavior of the functionally graded porous (FGP) doubly-curved panels and shells of revolution by using a semi-analytical method”, *Compos. Part B: Eng.*, **157**, 219-238. <https://doi.org/10.1016/j.compositesb.2018.08.087>